Acta Crystallographica Section D
**Biological Crystallography**
ISSN 0907-4449

# A crystallographic fragment screen identifies cinnamic acid derivatives as starting points for potent Pim-1 inhibitors

**Michèle N. Schulz,‡ Jörg Fanghänel, Martina Schäfer, Volker Badock, Hans Briem, Ulf Boemer, Duy Nguyen, Manfred Husemann and Roman C. Hillig***

Bayer Schering Pharma AG, Global Drug Discovery, Berlin 13342, Germany

‡ Present address: YSBL, University of York, York YO10 5DD, England.

Correspondence e-mail: roman.hillig@bayer.com

Received 20 November 2010
Accepted 24 December 2010

**PDB References:** Pim-2–inhibitor complexes, 2xix; 2xiy; 2xiz; 2xj0; 2xj1; 2xj2.

A crystallographic fragment screen was carried out to identify starting points for the development of inhibitors of protein kinase Pim-1, a potential target for tumour therapy. All fragment hits identified *via* soaking in this study turned out to bind to the unusually hydrophobic pocket at the hinge region. The most potent fragments, two cinnamic acid derivatives (with a best $IC_{50}$ of 130 $\mu M$), additionally form a well defined hydrogen bond. The balance between hydrophobic and polar interactions makes these molecules good starting points for further optimization. Pim-2 inhibitors from a recently reported high-throughput screening campaign also feature a cinnamic acid moiety. Two of these Pim-2 inhibitors were synthesized, their potencies against Pim-1 were determined and their cocrystal structures were elucidated in order to determine to what degree the binding modes identified by fragment screening are conserved in optimized inhibitors. The structures show that the cinnamic acid moieties indeed adopt the same binding mode. Fragment screening thus correctly identified binding modes which are maintained when fragments are grown into larger and higher affinity inhibitors. The high-throughput screening-derived compound (*E*)-3-{3-[6-(4-aminocyclohexylamino)-pyrazin-2-yl]phenyl}acrylic acid (compound 1) is the most potent inhibitor of the cinnamic acid series for which the three-dimensional binding mode is known ($IC_{50}$ = 17 n$M$, $K_d$ = 28 n$M$). The structure reveals the molecular basis for the large gain in potency between the initial fragment hit and this optimized inhibitor.

## 1. Introduction

Since its first application in 1996 (Shuker *et al.*, 1996), fragment-based lead discovery (FBLD) has developed into a powerful tool for drug discovery. Fragment screening is now integrated into the drug-discovery pipelines of most pharmaceutical companies and many academic groups have also reported successful ligand discovery *via* this method (Congreve *et al.*, 2008; Fischer & Hubbard, 2009; Schulz & Hubbard, 2009). We have carried out a crystallographic fragment screen with a small focused library for the ATP-binding site of protein kinases to analyze the suitability of this method for the protein kinase Pim-1. Protein kinases share a common fold, with an N-terminal lobe mainly consisting of $\beta$-strands and a C-terminal lobe formed mainly by $\alpha$-helices (Knighton *et al.*, 1991; Fig. 1). ATP is coordinated in a deep and narrow binding pocket at the hinge which connects the two lobes. The substrate peptide is coordinated in a more open and shallow binding site mainly located on the C-terminal lobe (Bullock, Debreczeni, Amos *et al.*, 2005). The kinase ATP-binding site and subpockets in its immediate vicinity are important target sites for small-molecule inhibitors. A number of such inhibi-

tors are now approved as drugs or are in clinical studies (Johnson, 2009). Pim-1 (proviral insertion site in Moloney murine leukaemia virus, isoform 1) is a serine/threonine protein kinase which was originally identified as a common integration site in Moloney murine leukaemia virus (MMLV)-induced T-cell lymphomas (Cuypers *et al.*, 1984). Pim-1 has been described as a possible target for cancer therapy; it is overexpressed in several cancers, such as prostate cancer and lymphomas (Dhanasekaran *et al.*, 2001; Valdman *et al.*, 2004; Cuypers *et al.*, 1984), and acts as a proto-oncogene (van Lohuizen *et al.*, 1989; Breuer *et al.*, 1989) and a survival factor (Lilly & Kraft, 1997). The human Pim kinase family consists of three isoforms, Pim-1, Pim-2 and Pim-3, all of which feature a unique hinge region with the motif $^{120}$LERP*X*P*X*$^{126}$ (with amino acids in single-letter code, numbering given for isoform Pim-1 and with Leu120 representing the gatekeeper residue). Crystal structures of Pim-1 (Bullock, Debreczeni, Amos *et al.*, 2005; Bullock, Debreczeni, Fedorov *et al.*, 2005; Jacobs *et al.*, 2005; Kumar *et al.*, 2005; Qian, Wang *et al.*, 2005; Shafer *et al.*, 2008; Cheney *et al.*, 2007; Pagano *et al.*, 2007) and Pim-2 have been determined (Bullock *et al.*, 2009). Compared with other kinases, the hinge region of Pim kinases features a one-amino-acid insertion after Pro123 which causes it to bulge out from the ATP-binding site (Jacobs *et al.*, 2005; Kumar *et al.*, 2005; Qian, Wang *et al.*, 2005). In addition, the presence of Pro123 at the hinge changes the potential interaction pattern with inhibitors, as proline cannot donate a hydrogen bond to the ligand (Jacobs *et al.*, 2005; Kumar *et al.*, 2005).

Our crystallographic fragment screen with Pim-1 identified several fragment binders, including two cinnamic acid derivatives. In addition, we generated crystal structures of Pim-1 in complex with two members of a Pim-2 inhibitor series which feature the same moiety and were recently discovered independently *via* high-throughput screening (HTS; Morwick *et al.*, 2008; Qian *et al.*, 2009). We discuss the results of our fragment-screening study and compare the binding modes of the cinnamic acid fragment hits with the optimized Pim-2 compounds originating from the HTS approach.

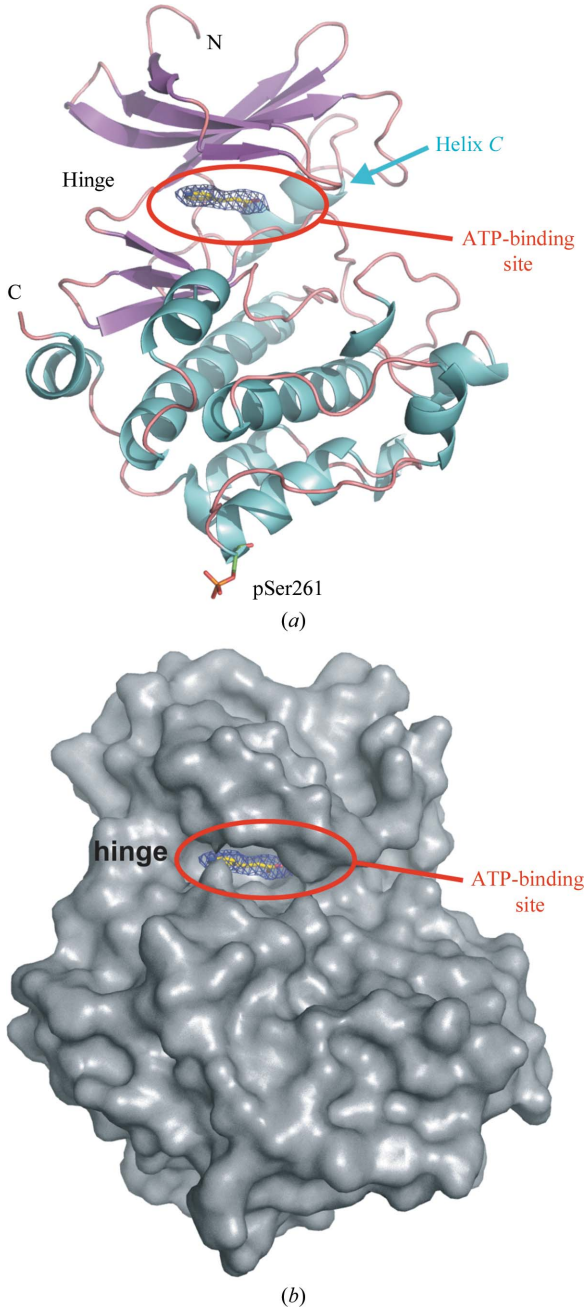


**Figure 1**
(*a*) Overall fold of the protein kinase Pim-1 in ribbon representation ($\alpha$-helices in blue, $\beta$-strands in purple, loops in orange) with fragment 3 bound in the ATP site at the hinge region shown as $2F_o - F_c$ density contoured at 1.0$\sigma$. The phosphorylated Ser261 is shown in stick representation. (*b*) Overall molecular surface, illustrating the deep ATP-site cavity.

## 2. Materials and methods

### 2.1. Cloning, expression, purification and crystallization

A Pim-1 construct comprising residues 14–313 based on the proteolytically stable domain reported by Qian, Studts *et al.* (2005) was cloned by Proteros Biosciences (Munich, Germany) and expressed in *Escherichia coli*. The protein was purified *via* nickel-affinity chromatography (HisTrap HP 5 ml, GE Healthcare) followed by tag cleavage and gel filtration (Superdex 200 HiLoad 26/60, GE Healthcare). Pim-1 aliquots were flash-frozen and stored at 193 K. Well diffracting rod-shaped hexagonal apo crystals of Pim-1 were obtained under the conditions reported previously by Jacobs *et al.* (2005). In brief, crystals were grown at 293 K using the hanging-drop method with 1 µl protein solution (4.5–6.3 mg ml$^{-1}$ in 200 m*M* NaCl, 50 m*M* HEPES pH 7.8, 5 m*M* $\beta$-mercaptoethanol) and 1 µl 0.7–1.0 *M* $(NH_4)_2HPO_4$, 200 m*M* NaCl, 100 m*M* sodium citrate pH 5.25–6.00. After two weeks, the hexagonal rod-shaped crystals reached final dimensions of 50–100 × 700 µm.

### 2.2. Mass spectrometry (MS)

Coomassie-stained Pim-1 bands were in-gel digested with trypsin (Promega). Tryptic peptides were directly analyzed by LC-ESI-MS/MS and phosphorylated peptides were enriched using $TiO_2$ tips (Glygen) and analyzed by MALDI-MS. LC-ESI-MS/MS experiments were performed on a QSTAR

**Table 1**
Molecular weight, $IC_{50}$ value and binding efficiency index (BEI) of the Pim-1 ligands analyzed in this study.

Structures are shown in Fig. 2.

| Name | Molecular weight (Da) | $IC_{50}$, Pim-1 activity assay (μ*M*) | BEI |
|---|---|---|---|
| Fragment 1 | 99 | >5000 | n.a. |
| Fragment 2 | 148 | 3600 | 16.5 |
| Fragment 3 | 149 | 130 | 26.1 |
| Fragment 4 | 165 | 1500 | 17.1 |
| Compound 1 | 338 | 0.017 | 23.0 |
| Compound 2 | 338 | 0.200 | 19.8 |

XL hybrid quadrupole-TOF instrument (AB/MDS Sciex) connected to an Eksigent nanoHPLC system and MALDI-MS and MS/MS experiments were performed on a MALDI-TOF/TOF 4700 Proteomics Analyzer (Applied Biosystems). Spectra were searched against an in-house database using the *Mascot* search engine (Matrix Science).

### 2.3. Chemistry

Compounds 1 and 2 (Table 1; Fig. 2) were synthesized as described by Morwick *et al.* (2008).

### 2.4. Fragment-library design and setup

A small focused library (148 compounds) for the ATP site of protein kinases (average molecular weight 162 Da) was assembled from two different sources: a scaffold library for kinase ATP-site motifs (Stahura *et al.*, 1999) and a set of compounds from a database of 90 000 compounds (average MW 250 Da) from the Available Chemicals Directory (ACD; Symyx Technologies, Sunnyvale, California, USA) selected based on docking studies in Cdk2 structures. Docking was carried out using *LUDI* (Böhm, 1992*a*,*b*) and *FlexX* (Rarey *et al.*, 1996) with constraints on the hinge region. For crystallographic screening, the library was sorted into 37 cocktails of four shape-diverse fragments (compounds with one-ring, two-ring and three-ring aromatic systems and a fourth compound which, based on its substitution pattern, could easily be differentiated from the other three). 500 m*M* stock solutions of each fragment were set up in DMSO and four such solutions were mixed (125 m*M* for each fragment) to form one fragment cocktail for crystal soaking.

### 2.5. Fragment soaking, data collection and structure determination

In this pilot study, only nine of the 37 cocktails of the focused fragment library were used for soaking experiments with Pim-1 crystals. 0.25 µl of a cocktail was added to a 1 µl drop containing Pim-1 apo crystals and incubated at 293 K for 24 h, resulting in a final concentration of 25 m*M* for each fragment. For single-fragment soaks, the stock solution was diluted to 125 m*M* in DMSO and 0.25 µl was added to a 1 µl drop. For compounds 1 and 2, 100 m*M* stock solutions in DMSO were diluted 1:5 with mother liquor, added to Pim-1 crystals (final concentration 6 m*M*) and incubated for 24 h. All crystals were flash-frozen in mother liquor supplemented with 30% glycerol and 1 m*M* ligand. X-ray diffraction data were collected at BESSY (Berlin, Germany) at 100 K (λ = 0.91841 Å, MAR CCD detector). Data were processed with *HKL*-2000 (Minor *et al.*, 2006) and phases were determined by rigid-body refinement using *REFMAC*5 (Murshudov *et al.*, 1997) from the *CCP*4 program suite (Collaborative Computational Project, Number 4, 1994) with an in-house structure of Pim-1 as the starting model (for further details, see Table 2). This crystal form has also been reported from different crystallization conditions (Bullock, Debreczeni, Amos *et al.*, 2005; Bullock, Debreczeni, Fedorov *et al.*, 2005; Jacobs *et al.*, 2005; Kumar *et al.*, 2005; Qian, Wang *et al.*, 2005; Shafer *et al.*, 2008; Cheney *et al.*, 2007; Pagano *et al.*, 2007). Refinement and rebuilding was carried out with *REFMAC*5 and *Coot* (Emsley & Cowtan, 2004), except for fragment 4, where initially *CNX* (Accelrys Inc., San Diego, California, USA) and subsequently *REFMAC*5 were used for refinement. For this data set, the geometry restraints were tightened because of the lower resolution. Several refinement cycles were carried out before the ligand was placed. The ligands were built using *Discovery Studio* (Accelrys Inc., San Diego, California, USA) and parameters were calculated using *PRODRG* (Schüttelkopf & van Aalten, 2004). The density next to fragment 2 (Fig. 3*b*) was modelled as a chloride ion from the crystallization buffer because an alternatively placed water molecule showed remaining difference density and a very low *B* factor. The diffraction images for fragment 3 showed ice rings owing to a suboptimal cryobuffer. This was

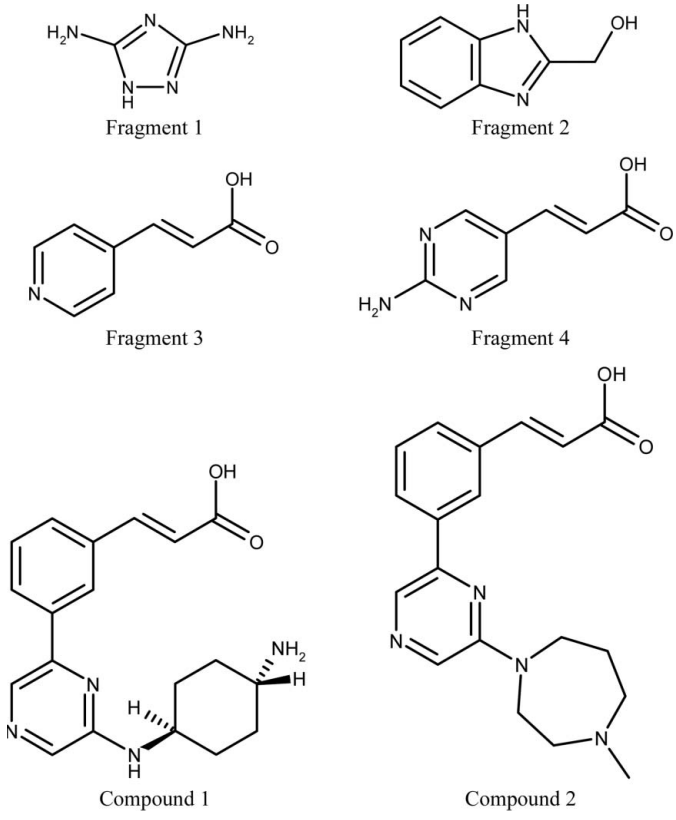


**Figure 2**
Structures of the ligands analyzed in this study.

**Table 2**
Data-processing and refinement statistics.

Values in parentheses are for the highest resolution shell.

| Ligand | Fragment 1 | Fragment 2 | Fragment 3 | Fragment 4 | Compound 1 | Compound 2 |
|---|---|---|---|---|---|---|
| PDB code | 2xix | 2xiy | 2xiz | 2xj0 | 2xj1 | 2xj2 |
| Complex formation | Single soak | Single soak | Cocktail soak | Single soak | Soak | Soak |
| Data processing | | | | | | |
| Space group | $P6_5$ | $P6_5$ | $P6_5$ | $P6_5$ | $P6_5$ | $P6_5$ |
| Unit-cell parameters (Å) | | | | | | |
| *a* | 96.8 | 97.0 | 96.8 | 96.2 | 95.8 | 96.2 |
| *c* | 80.6 | 80.9 | 80.7 | 80.5 | 80.9 | 80.8 |
| BESSY beamline | BL 14.2 | BL 14.2 | BL 14.1 | BL 14.2 | BL 14.2 | BL 14.2 |
| Resolution (Å) | 42.1–2.4 (2.49–2.40) | 48.6–2.2 (2.28–2.20) | 41.6–2.2 (2.30–2.20) | 42.1–3.1 (3.18–3.10) | 48.6–2.1 (2.21–2.13) | 41.6–2.2 (2.27–2.20) |
| Unique reflections | 15473 (869) | 21175 (1548) | 20132 (918) | 7338 (341) | 22397 (1472) | 21150 (1557) |
| Multiplicity | 6.9 (3.8) | 8.6 (4.8) | 8.0 (6.5) | 8.7 (5.2) | 9.0 (4.4) | 10.5 (6.2) |
| Completeness (%) | 91.2 (51.2) | 96.0 (71.3) | 91.6 (58.6) | 93.8 (61.8) | 94.8 (63.1) | 97.7 (80.3) |
| $\langle I/\sigma(I)\rangle$ | 17.2 (2.1) | 21.2 (2.3) | 26.4 (6.3) | 13.2 (2.1) | 35.4 (3.1) | 23.4 (2.6) |
| $R_{\rm merge}$† (%) | 10.0 (44.2) | 8.9 (44.6) | 6.0 (25.8) | 15.6 (52.1) | 5.6 (31.8) | 9.6 (47.9) |
| Refinement | | | | | | |
| Reflections (work/test) | 14680/780 | 20074/1065 | 18504/982 | 6951/364 | 21246 /1123 | 20051/1067 |
| $R_{\rm work}$‡ (%) | 17.1 | 17.0 | 25.6 | 21.6 | 17.6 | 16.7 |
| $R_{\rm free}$§ (%) | 21.4 | 20.1 | 28.6 | 26.3 | 21.2 | 20.2 |
| *B* factors (Å$^2$) | | | | | | |
| Overall | 22.0 | 18.2 | 39.2 | 49.7 | 52.5 | 24.3 |
| Protein | 22.2 | 18.2 | 40.0 | 49.7 | 52.7 | 24.4 |
| Ligand | 35.8 | 18.3 | 29.2 | 58.6 | 47.4 | 16.6 |
| Water | 15.7 | 17.7 | 14.3 | 31.5 | 49.0 | 24.2 |
| Chloride/glycerol | — | 38.4 | — | — | — | — |
| R.m.s.d. bond lengths (Å) | 0.012 | 0.010 | 0.008 | 0.002 | 0.011 | 0.010 |
| R.m.s.d. bond angles (°) | 1.415 | 1.214 | 1.123 | 0.727 | 1.246 | 1.200 |
| Ramachandran plot | | | | | | |
| Preferred regions | 252 [95.5%] | 253 [96.9%] | 241 [91.2%] | 252 [93.0%] | 263 [97.4%] | 257 [97.0%] |
| Additionally allowed | 9 [3.4%] | 6 [2.3%] | 18 [6.9%] | 14 [5.2%] | 5 [1.9%] | 6 [2.3%] |
| Outliers | 3 [1.1%] | 2 [0.8%] | 3 [1.2%] | 5 [1.9%] | 2 [0.8%] | 2 [0.8%] |

† $R_{\rm merge} = \sum_{hkl}\sum_i |I_i(hkl) - \langle I(hkl)\rangle| / \sum_{hkl}\sum_i I_i(hkl)$, where $I_i(hkl)$ is the intensity of a single reflection and $\langle I(hkl)\rangle$ is the average intensity of the same reflection. ‡ *R* factor = $\sum_{hkl} ||F_{\rm obs}| - |F_{\rm calc}|| / \sum_{hkl} |F_{\rm obs}|$, where $F_{\rm obs}$ are the observed structure factors and $F_{\rm calc}$ are the calculated structure factors § In all data sets the same 5% of reflections were used to calculate $R_{\rm free}$.

probably responsible for the elevated *R* and $R_{\rm free}$ factors for this data set (Table 2). Figures were generated using *PyMOL* (v.1.3; Schrödinger) and *Discovery Studio* (Accelrys Inc., San Diego, California, USA).

### 2.6. Kinase activity assay and isothermal titration calorimetry (ITC)

3 µl Pim-1 kinase (Millipore, Dundee, Scotland; ∼0.5 pg per measurement point) was pre-incubated in assay buffer [25 m*M* HEPES pH 7.5, 10 m*M* $MgCl_2$, 1.0 m*M* dithiothreitol, 0.015% NP40, 0.01%(*w*/*v*) bovine serum albumin, Complete EDTA-free protease-inhibitor cocktail (Roche, one tablet per 2.5 ml), 0.1 m*M* $Na_3VO_4$] for 15 min with 50 nl of test compound dissolved in 100% DMSO in 384-well plates. The kinase reaction was started by the addition of 2 µl substrate solution [10 µ*M* ATP (approximately the apparent $K_m$) and 1 µ*M* peptide substrate (biotin-Ttds-YRRRHLSFAEPG-$NH_2$) dissolved in assay buffer] and terminated after 20 min at 295 K by the addition of 2 µl 0.25 *M* EDTA followed by the addition of 3 µl of an aqueous buffer [50 m*M* HEPES pH 7.5, 0.1%(*w*/*v*) BSA, 400 m*M* KF] which contained an antiphosphoserine antibody (1.5 n*M*; Millipore, Dundee, Scotland) and the homogenous time-resolved fluorescence (HTRF) detection reagents $Eu^{3+}$ cryptate-conjugated rabbit anti-mouse IgG (0.75 n*M*) and streptavidin-XLent! (0.05 µ*M*) (CisBio International, Marcoule, France). After complex formation, the fluorescence emissions at 665 and 620 nm (internal Eu reference signal) following excitation at 350 nm were measured in an HTRF reader (Rubystar, BMG Labtechnologies, Offenburg, Germany). The ratio of the emissions at 665 and 620 nm was taken as a measure of the amount of phosphorylated substrate peptide. $IC_{50}$ values were calculated by a four-parameter fit using in-house software.

ITC data were collected on an ITC 200 microcalorimeter (MicroCal) at 298 K. Experiments were performed in 50 m*M* Tris–HCl pH 7.8, 200 m*M* NaCl and 1 m*M* TCEP. Complex formation between Pim-1 and compounds 1 and 2 was characterized by titrating 99 µ*M* Pim-1 solution into a 20 µ*M* compound solution. Manual baseline and heat of dilution corrections were performed prior to data analysis. Thermodynamic parameters were obtained by employing the 'one-site' binding model included in the data-analysis package supplied by the manufacturer of the instrument. Table 3 shows the average values from three titration runs.

## 3. Results

### 3.1. Crystallographic fragment screening

In a technical feasibility study, a small focused library of 148 compounds for the kinase ATP site was designed. Cocktails

containing four shape-diverse fragments were set up. More than 30% of the 148 fragment stock solutions (500 m*M*) and also 30% of the cocktails were not fully soluble and were set up as suspensions. For the fragment screen with Pim-1, nine of the 37 cocktails (comprising a total of 9 × 4 = 36 fragments) were selected based on *in silico* docking (data not shown) and used in this study for soaking experiments. In some experiments, the harsh conditions (25 m*M* of each fragment, 20% DMSO) resulted in broken and bent crystals. However, in most cases the crystals survived and generally diffracted to between 2.0 and 3.1 Å resolution.

### 3.2. Overall structure of Pim-1

Pim-1 shows the typical bilobal fold of a protein kinase (Fig. 1), with an N-terminal lobe mainly consisting of $\beta$-sheets and a C-terminal lobe mainly formed by $\alpha$-helices. The cleft between the two lobes harbours the ATP-binding site. In all fragment co-complex structures reported here Pim-1 is in the active conformation as judged from the DFG-in conformation and from the presence of the typical salt bridge between Lys67 in the ATP site and Glu89 from helix *C*.

**Table 3**
ITC-derived thermodynamic parameters for compounds 1 and 2.

1 kcal = 4.186 kJ.

| | $\Delta G_{ITC}$ (kcal mol$^{-1}$) | $\Delta H_{ITC}$ (kcal mol$^{-1}$) | $-T\Delta S_{ITC}$ (kcal mol$^{-1}$) | $K_d$ (n*M*) |
|---|---|---|---|---|
| Compound 1 | −10.3 | −8.9 ± 0.7 | −1.4 ± 0.8 | 28 ± 7 |
| Compound 2 | −9.8 | −9.2 ± 0.2 | −0.6 ± 0.3 | 66 ± 8 |

MS analysis indicated phosphorylation at Ser97, Ser189 and Ser261 during *E. coli* expression. This was initially observed by intact mass determination and the sites were subsequently identified *via* in-gel digestion experiments. Since *E. coli* does not have endogenous serine/threonine kinases, these modifications are most likely to result from autophosphorylation and are probably artefacts from overexpression of the kinase. Separation *via* anion-exchange chromatography did not further improve crystallization; thus, the heterogeneously phosphorylated Pim-1 sample was ultimately used for crys-

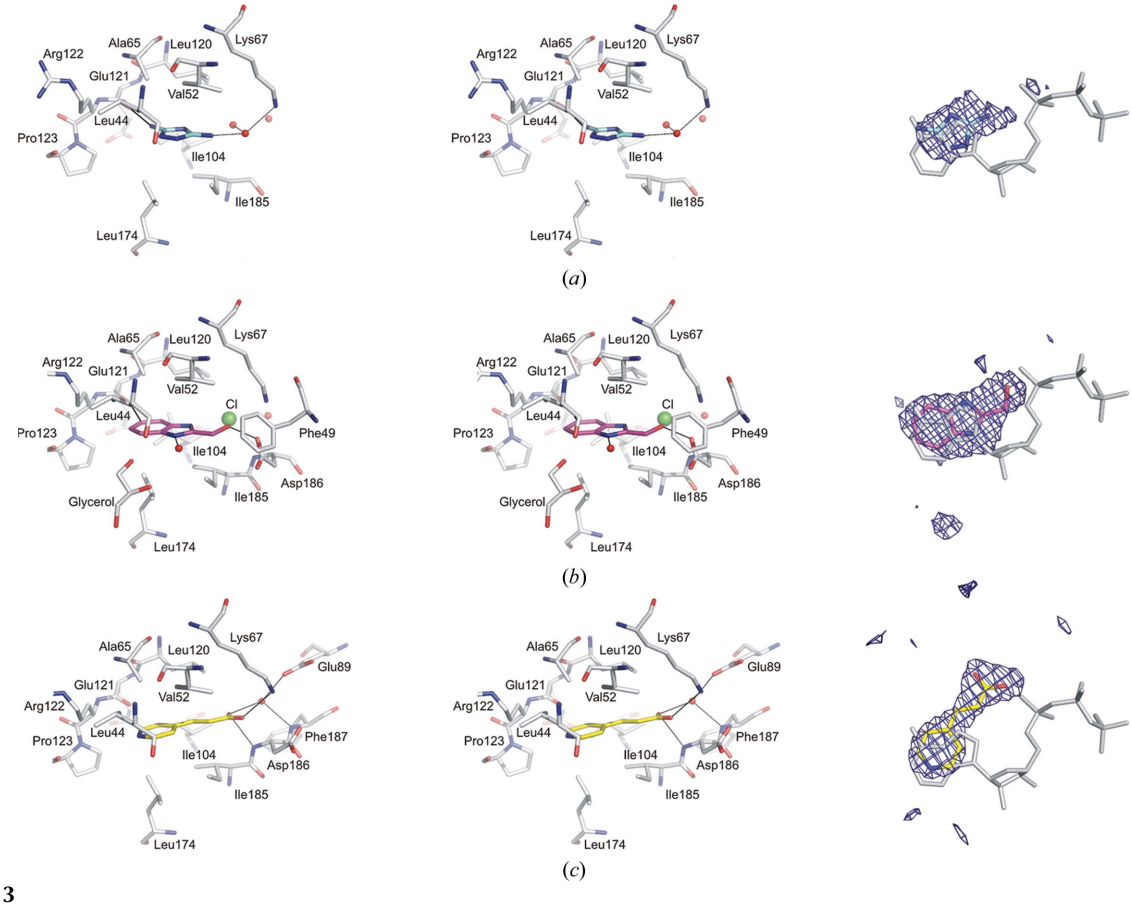


**Figure 3**
Stereo representation of the binding modes of the fragments and inhibitors in the ATP-binding site of Pim-1: (*a*) fragment 1 (C atoms in cyan), (*b*) fragment 2 (magenta), (*c*) fragment 3 (yellow), (*d*) fragment 4 (pink), (*e*) compound 1 (green) and (*f*) compound 2 (orange). The ligands and the Pim-1 residues within a 4 Å distance of the ligand are shown in stick representation. For orientation, the right side of each panel shows the respective ligand and the ATP derivative AMPPNP (from a superimposition of the protein chain with PDB entry 1xr1; AMPPNP is shown in grey). The orientation on the right side is rotated by approximately 90° compared with the left side around a horizontal axis to allow a view perpendicular to the aromatic ring system of the adenine base. The electron-density maps are $F_o - F_c$ omit maps calculated from the final model from which the ligand was omitted (contoured at 3$\sigma$ and truncated at a distance of 4 Å from the ligand), except for fragment 4 where the final $2F_o - F_c$ omit map is shown (contoured at 0.8$\sigma$ and truncated at 2 Å around the ligand).

tallization. The electron-density maps consistently indicated phosphorylation at Ser261 only, which has been described as an artefact from *E. coli* expression (Bullock, Debreczeni, Amos *et al.*, 2005). Only the structure with fragment 1 showed density for additional phosphorylation at Ser276. Both sites are distant from the ATP site (37 and 34 Å, respectively) and are thus not expected to affect inhibitor binding. The three new autophosphorylation sites identified by MS (Ser97, LLKKVSS, Ser189, LIDFGSG, and Ser276, LALRPSD) do not closely resemble the Pim-1 consensus motif RRRHPSG, as reported by Bullock, Debreczeni, Fedorov *et al.* (2005). Ser97 and Ser189 do not directly contribute to the ATP site either (11 and 9 Å distance, respectively) and are therefore also not expected to affect the binding of an inhibitor to the ATP site. Ser189 is located in the activation segment ($^{186}$DFG . . . PPE$^{211}$).

### 3.3. Fragment-binding modes

After soaking Pim-1 crystals with nine different fragment cocktails, all structures featured electron density for a bound fragment in the ATP site. However, only four of the initial nine data sets allowed unambiguous identification of the bound fragment. For the remaining data sets, single-fragment soaking experiments were carried out. A total of 12 fragment hits were identified in this crystallographic screen of 36 compounds. For four of these the $IC_{50}$ values in a protein kinase activity assay were below 10 m*M* and could be determined (Table 1). The binding modes of these four best fragment hits will be discussed in detail in the following. The final electron-density omit maps for these fragment hits are shown in Fig. 3, together with the ATP derivative AMPPNP as derived from a superimposition with the structure of Pim1–AMPPNP (PDB code 1xr1; Qian, Wang *et al.*, 2005).

Fragment 1 (3,5-diamino-1H-1,2,4-triazole; Table 1; Fig. 2) binds solely within the adenine subpocket and mimics the five-membered ring of adenine (Fig. 3*a*). Both amino groups of this fragment form polar interactions with Pim-1: a direct hydrogen bond (3.2 Å) to the carbonyl group of Glu121 from the hinge region and a water-mediated hydrogen bond to the conserved Lys67 at the back of the ATP site (ligand–water and water–protein distances of 2.4 and 2.9 Å, respectively). In addition, the fragment is hydrophobically coordinated by Ala65, Ile185, Ile104, the gatekeeper Leu120 and Leu174. In a Pim-1 kinase activity assay fragment 1 showed signs of inhi-

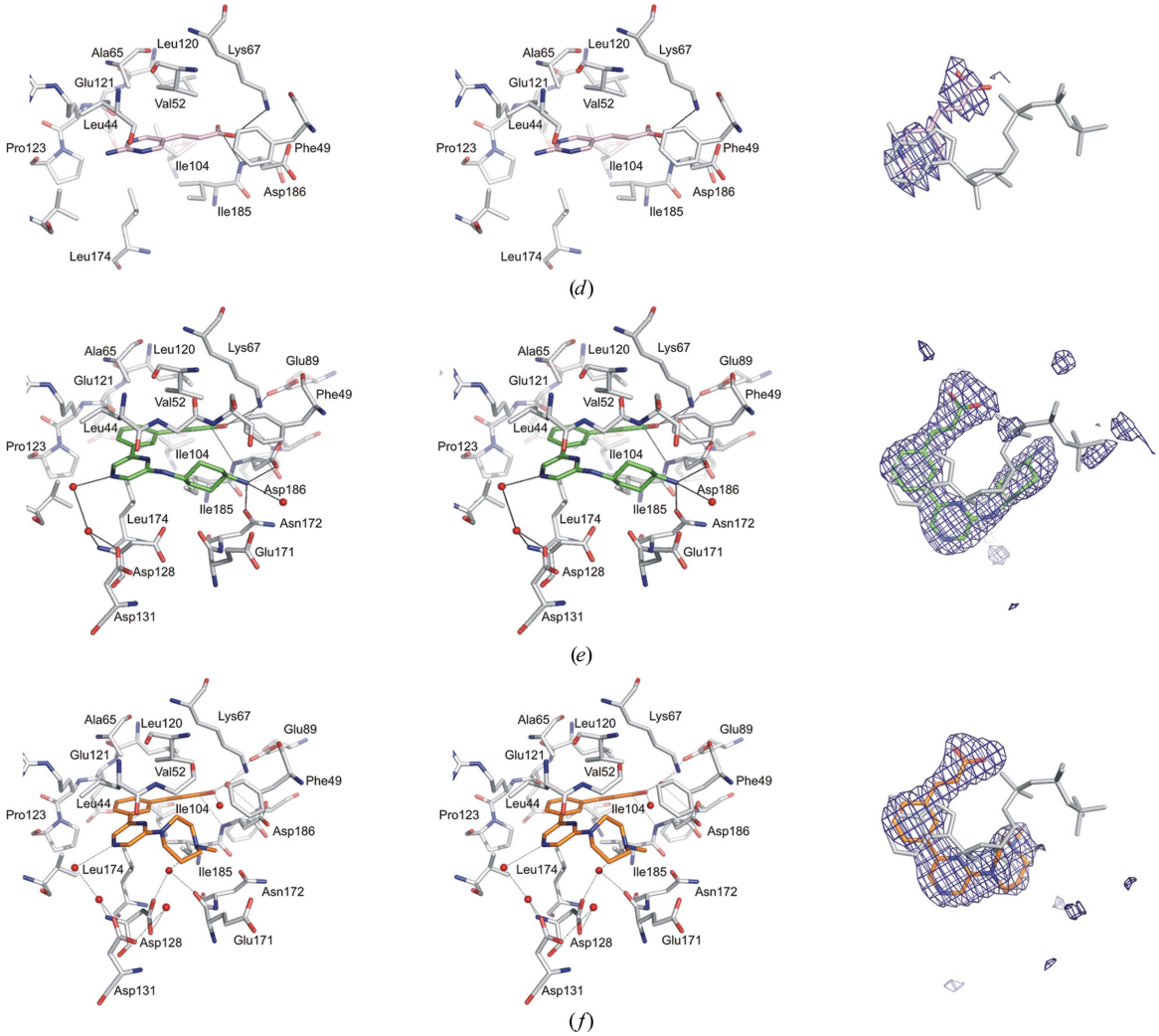


**Figure 3 (continued)**

bition, but the inhibition was not saturated at the maximal concentrations used in the assay. The $IC_{50}$ was therefore only estimated to be weaker than 5 m*M*.

Fragment 2 (2-hydroxymethylbenzoimidazole) also binds within the adenine subpocket of the ATP site and mimics both rings of the adenine moiety (Fig. 3*b*). It forms a weak C—H···O hydrogen bond (Weiss *et al.*, 2001) to Glu121 (3.3 Å). The hydroxyl group points towards the $\alpha$-phosphate subpocket in the ATP site and forms a direct hydrogen bond to the carboxyl side chain of Asp186 from the DFG motif (2.4 Å). Compared with Pim-1 in complex with the other ligands reported here, Asp186 adopts an alternative rotamer conformation in which its side chain is rotated towards the fragment. In addition to these polar interactions, fragment 2 is coordinated *via* extensive hydrophobic interactions with Leu44, Ala65, Val52, Ile104 and Leu174. A chloride ion, which is most likely to originate from the mother liquor, binds at the back of the ATP pocket, coordinated between the fragment, the gatekeeper Leu120, Ile104 and Lys67. This subpocket is occupied by a conserved water molecule in most of our fragment structures. In addition, there is a glycerol molecule coordinated in front of the ATP pocket (Fig. 3*b*). It originates from the cryobuffer and forms hydrogen bonds to the backbone amide of Asp128 and the side chain of Asp131. Fragment 2 inhibits Pim-1 kinase activity with an $IC_{50}$ of 3.6 m*M* and a binding efficiency index (BEI; Abad-Zapatero & Metz, 2005) of 16.5 (Table 1).

The binding mode of the cinnamic acid derivative fragment 3 [(*E*)-3-pyridin-4-yl-acrylic acid] is shown in Fig. 3(*c*). The pyridine ring occupies the adenine pocket. It is coordinated *via* hydrophobic interactions with Leu44, Ala65 from the top of the ATP site, Leu174 (of the catalytic loop) from below, Ile104 from the back wall and the hydrophobic part of the side chain of Arg122 from the hinge region. The pyridine N atom is not involved in any polar interactions. The ethenyl linker group of fragment 3 is in hydrophobic contact with the gatekeeper Leu120 and Ile185. The carboxyl group is involved in a network of hydrogen-bond interactions: it forms a direct salt bridge (2.8 Å) to the $\varepsilon$-amino group of Lys67 at the back of the ATP-binding site and two water-mediated hydrogen bonds to the amide N atom of Phe187 of the DFG motif (ligand–water and water–protein distances of 2.8 and 2.8 Å, respectively) and to the carboxyl group of the conserved Glu89 from helix *C* (2.8 and 2.9 Å, respectively). The amide N atom of Asp186 forms an N—H···$\pi$ interaction with the carboxyl group of the fragment. With an $IC_{50}$ value of 130 $\mu M$ and a BEI of 26.1, fragment 3 is the most potent fragment identified in this screen.

The closely related cinnamic acid derivative fragment 4 [*E*-3-(2-amino-pyridin-5-yl)-acrylic acid; Fig. 3*d*] was identified in a structure derived from a lower resolution data set (Table 2). At 3.1 Å resolution, the placement of the fragment in the initial electron-density maps was additionally guided by inspection of the potential interaction patterns and by the binding mode observed with fragment 3. Fragment 4 has the same overall binding mode as fragment 3, with extensive hydrophobic interactions in the adenine subpocket and a salt bridge to Lys67. As with the pyridine moiety in fragment 3, the aminopyrimidine moiety is not involved in polar interactions with Pim-1. The $IC_{50}$ value for fragment 4 was 1.5 m*M* and thus is 12-fold weaker than for the very similar fragment 3. This decrease in potency may be caused either by a less optimal fit of the aminopyrimidine moiety or by different desolvation effects upon binding to the ATP site.

### 3.4. Two Pim-2 inhibitors with cinnamic acid groups: binding modes and thermodynamic characterization in Pim-1

We also determined the structures of Pim-1 in complex with two aminopyrimidine compounds which have been reported to be Pim-2 inhibitors (Morwick *et al.*, 2008) and which feature a cinnamic acid moiety (compounds 1 and 2; Table 1; Fig. 2).

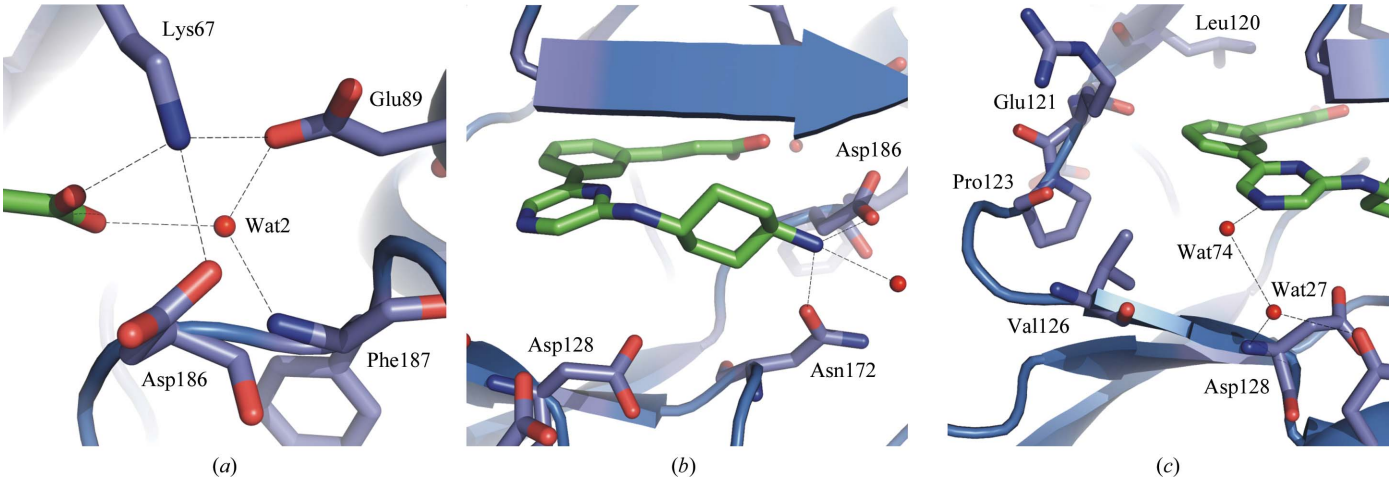


**Figure 4**
Detailed presentation of the binding mode of compound 1. Pim-1 is shown in blue and the C atoms of the ligand are depicted in green. The ligand and selected protein residues are shown in stick representation and hydrogen bonds are depicted as dotted lines. (*a*) The hydrogen-bonding network coordinating the carboxyl head group of the cinnamic acid moiety. (*b*) Interactions between the outer amino group of the ligand and Pim-1. (*c*) Interactions between the hinge region and the ligand.

Figs. 3(*e*) and 3(*f*) show the binding modes and the well defined electron-density omit maps for both compounds. The binding mode of compound 1 is presented in more detail in Fig. 4. Neither of the compounds adopt the canonical binding mode of aminopyrimidines to kinase ATP sites, *i.e.* with the pyrimidine ring occupying the adenine subpocket and the formation of two hydrogen bonds to the hinge region (see, for example, Lucking *et al.*, 2007). Instead, the phenyl ring of the cinnamic acid moiety occupies the adenine subpocket and binds in the same mode as observed for fragments 3 and 4 (Fig. 4*a*). The pyrimidine rings of both compounds extend from the adenine pocket into the hydrophobic pocket at the entrance of the ATP site and are sandwiched between Leu44 and Leu174. The outer cyclohexylamino moiety of compound 1 folds back towards the cinnamic acid group, resulting in a horseshoe-shaped overall conformation (Fig. 4*b*). It is stabilized in this conformation *via* a 3.1 Å salt bridge from the amino group to the side chain of Asp186 and a 3.1 Å hydrogen bond to the side chain of Asn172. One N atom of the piperidine forms a hydrogen bond to the backbone amide of Asp128 which is mediated *via* two water molecules (Fig. 4*c*). In contrast to the fragment hits, Phe49 at the end of the P-loop has to move away in order to avoid a steric clash (Fig. 3*e*). It is poorly defined in the density and is probably flexible. Characterization by ITC (Fig. 5 and Table 3) reveals that binding to Pim-1 is predominantly driven by enthalpy. The $K_d$ of 28 n*M* is in good agreement with the $IC_{50}$ of 17 n*M* determined in the kinase-activity assay.

Compound 2 features a methyl-1,4-diazepane ring instead of the aminocyclohexyl moiety. It kinks down towards the floor of the ATP pocket and forms water-bridged hydrogen bonds to the backbone of Glu171 and the side chain of Asp128. The thermodynamic parameters show that binding is again driven by enthalpy. $\Delta H$ is comparable to that of compound 1. The overall $K_d$ (66 n*M*) is weaker than for compound 1, which is caused by a less favourable entropic contribution. This overall entropy reduction may be a result of reduced mobility of the P-loop. Phe49 from this loop does not need to move outwards. Its phenyl ring is well defined in the electron density owing to a van der Waals interaction with the diazepane moiety.

## 4. Discussion

The limited crystallographic fragment screen with Pim-1 and a small focused library for the ATP site of protein kinases resulted in a high number of hits (12 fragments bound out of 36 fragments tested). This may in part be explained by the fact

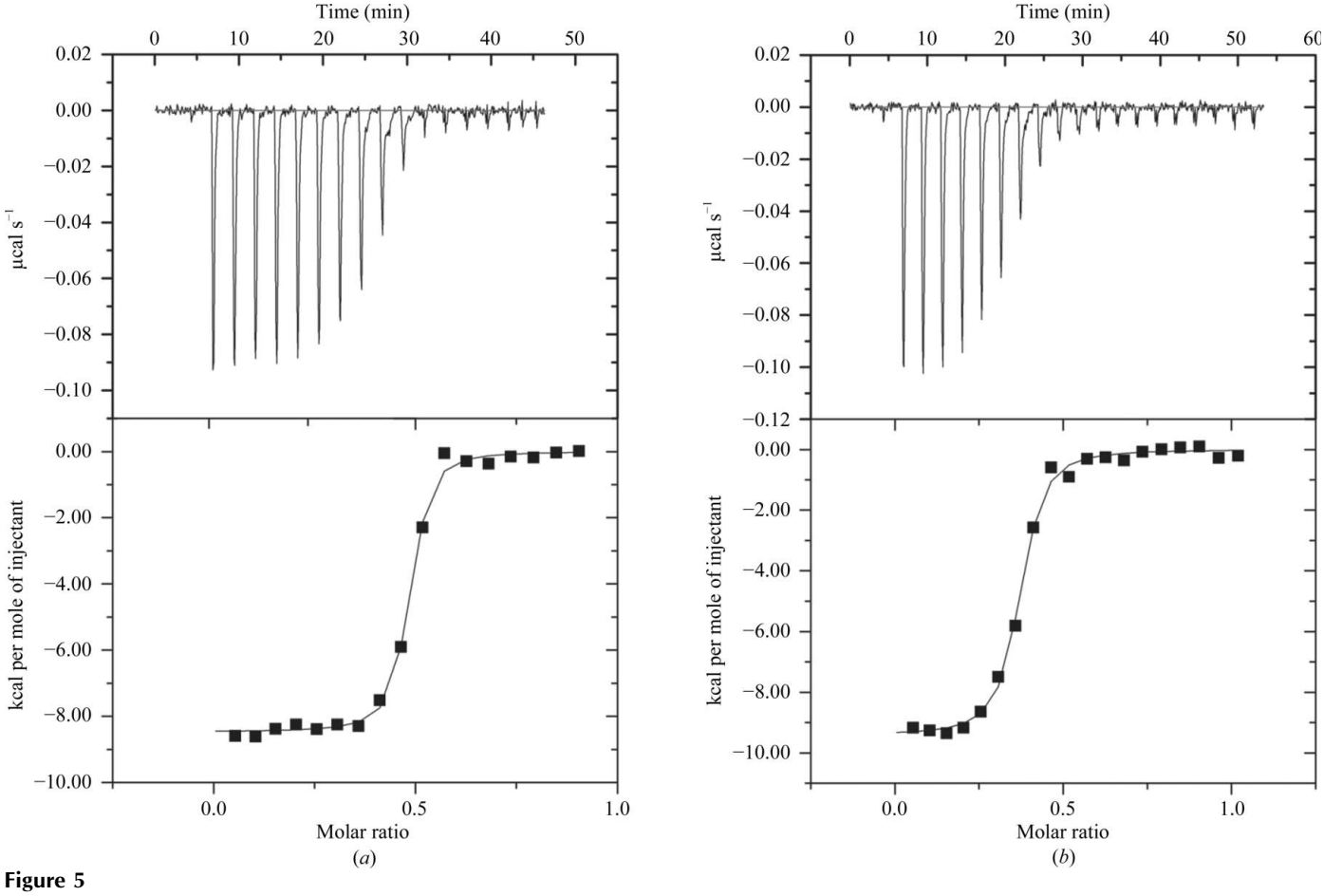


**Figure 5**
ITC data for the interaction of Pim-1 with (*a*) compound 1 and (*b*) compound 2. Representative raw data are shown in the upper panel. The lower panels show the heats of reaction normalized to the number of moles of Pim-1 injected (corrected for heat of dilution) and a nonlinear least-squares fit of the data. 1 cal = 4.186 J.

that the fragment library had been assembled with a strong bias for kinase ATP-site binders and the cocktails used had been prioritized *via* docking. In a crystallographic screen with Pim-1 using fragments which were pre-selected by a high-concentration screen, Kumar and coworkers also observed high hit rates (70 binders in 150 data sets; Kumar *et al.*, 2005). In an unprioritized crystallographic screen of a fragment library typical hit rates are only about 5%, while hit rates for kinases are typically higher (about 10%) but vary between different kinases (Bamborough *et al.*, 2008). The high ligand concentration (25 m*M*) used in this study is typical for crystallographic fragment screening (up to 50 m*M* per compound; Ciulli & Abell, 2007) and allowed the identification of low-potency binders such as fragment 1 with an $IC_{50}$ of above 5 m*M*. We also attribute the high success rate with Pim-1 to the fact that the adenine pocket of this kinase is unusually hydrophobic, which is caused by the inability of Pro123 in the hinge region to donate a hydrogen bond. The top four fragment hits presented here and also a further eight weaker binding hits (not shown) occupy the hydrophobic adenine subpocket within the ATP-binding site. This corresponds well to the observations of Kumar and coworkers, in which the majority of the 70 Pim-1 fragment hits were also found in the adenine subpocket (Kumar *et al.*, 2005).

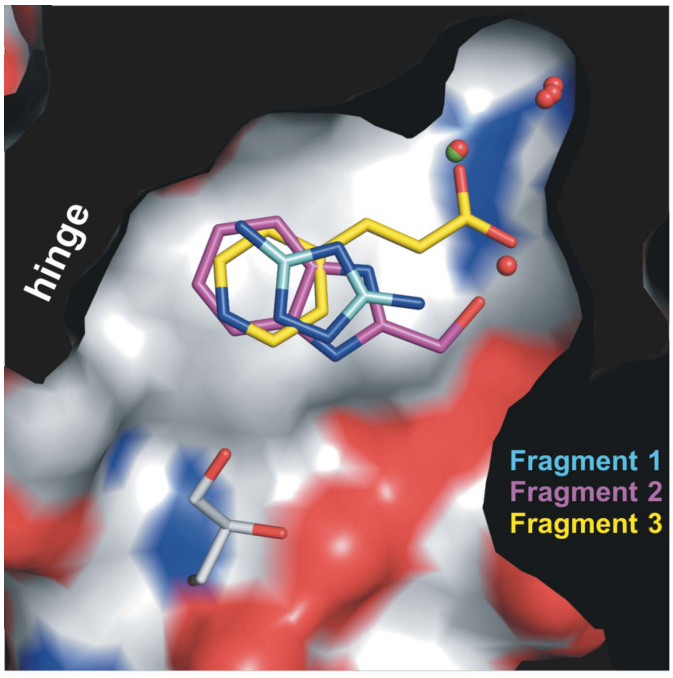


(*a*)

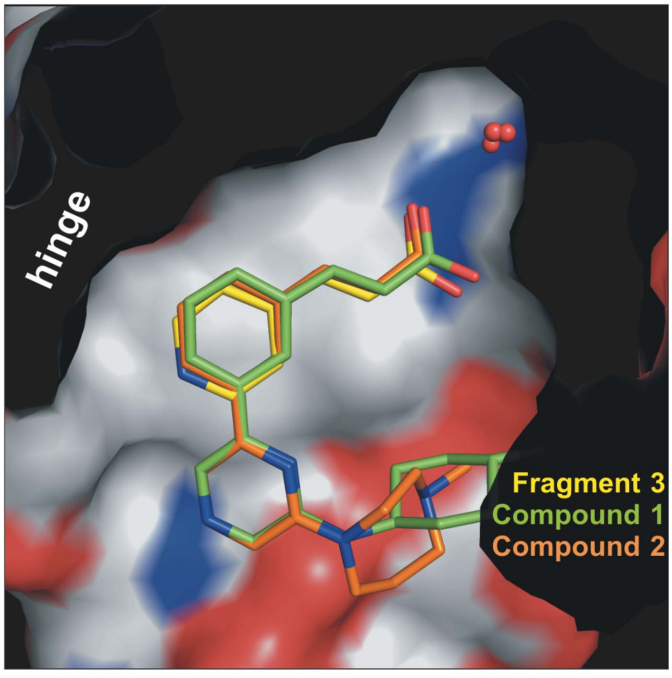


(*b*)

**Figure 6**
Cross-sections through the ATP-binding site of Pim-1. (*a*) Fragment 1 and fragment 2 superimposed onto fragment 3 (as derived from a superimposition of the protein chains), together with selected water molecules (red spheres) and a cocrystallized chloride ion (green sphere) and glycerol molecule (C atoms in white). (*b*) Compound 2 and fragment 3 superimposed onto compound 1. The protein surface is colour-coded according to electrostatic potential (red for negatively charged and blue for positively charged).

Hydrophobic interaction is often driven by entropy, as it results in changes in the solvation of hydrophobic groups upon formation of the complex (Olsson *et al.*, 2008 and references therein). Based on the outcome of our fragment screen and that of Kumar and coworkers, it appears to be straightforward to identify hydrophobic fragment hits for the hydrophobic adenine subpocket in the ATP site of Pim-1. Therefore, we considered those Pim-1 fragment hits which, in addition to hydrophobic interactions, already feature well defined polar interactions to be the best starting points for a fragment-to-lead optimization campaign. This strategy of combining a hydrophobic moiety with a polar anchor or 'warhead' was suggested by Geschwindner *et al.* (2007). Within our fragment hits, the two cinnamic acid derivatives fragments 3 and 4 are good examples of this approach as they extend from the hydrophobic adenine pocket towards the conserved Lys67 residue, where their carboxyl group forms several polar interactions. The superimposition shown in Fig. 6(*a*) reveals that the two O atoms of the carboxyl group of fragment 3 almost perfectly mimic and replace two ordered water molecules bound in the depth of the ATP pocket next to fragment 1, as well as an ordered chloride ion bound next to fragment 2. Replacement of these solvent molecules will add favourably to the entropic contribution of the free binding energy. With an $IC_{50}$ of 130 µ*M* and a binding efficiency index (BEI) of 26.1 [BEI = $pIC_{50}$/molecular weight (kDa); Abad-Zapatero & Metz, 2005], fragment 3 is also the most potent Pim-1 fragment identified here (Table 1).

After we had solved the structures of the cinnamic acid derivative fragments 3 and 4, we noticed similarity to an inhibitor series that had been identified in a high-throughput screen (HTS) with Pim-2 (Morwick *et al.*, 2008). To understand whether our fragment hits and the reported HTS hit series indeed feature the same overall binding mode with regard to the cinnamic acid moiety, we synthesized two members of this series as tool compounds and determined both the $IC_{50}$ values for inhibition of Pim-1 and the crystal structures of the com-

plexes with Pim-1. Although reported as Pim-2 inhibitors ($IC_{50}$ values of 150 n*M* for compound 1 and 40 n*M* for compound 2; Morwick *et al.*, 2008; Qian *et al.*, 2009), both compounds also potently inhibited Pim-1 in our kinase-activity assay, with $IC_{50}$ values of 17 n*M* for compound 1 and 200 n*M* for compound 2. This was not surprising as all residues lining the ATP-binding sites are conserved between Pim-1 and Pim-2 (Fedorov *et al.*, 2007). The crystal structures revealed that the cinnamic acid moiety of these optimized Pim-1/2 inhibitors indeed binds in the same way as seen with our fragment hits (Fig. 6*b*). The gain in potency from 130 µ*M* for fragment 3 to 17 n*M* for compound 1 can be interpreted as the result of the growth of the fragment hit *via* its aromatic ring towards the solvent: an additional pyrimidine ring in compounds 1 and 2 fills a hydrophobic pocket formed by Leu44 and Leu174 at the entrance of the ATP site, which is likely to add a favourable entropic contribution to the free binding energy. The aminocyclohexylamino moiety of compound 1 forms two additional polar interactions, while the outer diazepane ring of compound 2 generates one further hydrogen bond. Compared with the fragment hits, these additional polar contacts add favourably to the enthalpic part of the free binding energy.

Growing a fragment into a small-molecule inhibitor often decreases the binding efficiency index (BEI) as not all atoms added will contribute favourably to the binding affinity. This is illustrated by the drop in the BEI from 26.0 for fragment 3 to 23.0 and 19.8 for compounds 1 and 2, respectively (Table 1). Qian *et al.* (2009) provide an overview of known Pim-1 inhibitors and their binding affinities. These correspond to BEI values of 17.6–22.4. Fragment 3 thus represents an excellent Pim-1 binder and the related compound 1 is the most efficient Pim-1 small-molecule inhibitor reported to date.

While this manuscript was in preparation, the structure of Pim-1 in complex with compound 2 and a magnesium ion was published (Qian *et al.*, 2009). Superimposition of this structure and our structure shows a very good agreement for the protein (r.m.s.d. of 0.2 Å for all non-H atoms) and identical binding modes for the inhibitor. The only significant difference is a magnesium ion in the structure of Qian *et al.* (2009) which, based on the observed coordination distances, was modelled as a water molecule in our structure (wat2 in Fig. 4*a*).

In the complex of Pim-1 and fragment 2 a glycerol molecule from the cryobuffer was found in front of the ATP site, forming hydrogen bonds to Asp128 and Asp131. This cryoprotectant artefact can be considered as a second fragment hit, which reveals these two residues as possible further interaction points in the proximity of the ATP site. A Pim-1 inhibitor reported by Pierce *et al.* (2008) (PDB entry 3bgp) places a chlorophenyl moiety towards the glycerol subpocket, but is not able to form the two hydrogen bonds to Asp128 and Asp131. Our structure thus suggests a way to further optimize future Pim-1 inhibitors. Similarly, the chloride ion observed in the co-complex with fragment 2 indicates that in the back of the pocket a suitably positioned Cl atom could be incorporated into an inhibitor. A similar binding mode of a chloride ion in this position has also been observed in two Pim-1 crystal structures deposited by the Structural Genomics Consortium Oxford (PDB entries 3cxw and 3cy2). The exact chloride position differs by 1.3 Å from our position, most likely owing to a different rotamer of the adjacent Asp186 from the DFG motif.

All fragment hits identified in this crystallographic fragment screen bound in the adenine pocket at the hinge region. In all cases the kinase domain was in an active conformation as judged from the DFG-in conformation of the activation segment and the presence of a salt bridge between Glu89 from helix *C* and the conserved ATP-site lysine residue (Lys67). Although the hits revealed molecular interactions that will support further inhibitor design and optimization, it would have been even more desirable to identify fragments binding to other subpockets in or around the ATP site. This would reveal further directions in which initial hits from FBLD or high-throughput screening could be optimized. To identify such rarely occurring compounds would most likely require the screening of a much larger library of compounds. To prioritize the hits coming out of such a screen, a pre-X-ray filter may be an attractive additional step, in which a biophysical method (such as surface plasmon resonance, thermal shift assay or ligand-observed NMR) or high-concentration screening is used to identify fragment hits, which are then subsequently characterized by crystal structure analysis (Schulz & Hubbard, 2009). Compared with crystallographic screening *via* soaking, such a two-step approach may enable the identification of fragment binders which require a conformational change of the kinase domain to bind. In such cases cocrystallization experiments would be required to determine the cocomplex crystal structures.

The crystallographic fragment screen with protein kinase Pim-1 was able to identify both potent fragments (fragment 3, $IC_{50}$ = 130 µ*M*) and weak-affinity binders (fragment 1, $IC_{50}$ > 5 m*M*). In particular, it revealed cinnamic acid derivatives as binders for the ATP site of Pim-1. They represent starting points for a fragment-based lead-discovery approach as they form both hydrophobic interactions and a well defined polar interaction with the ATP site. The elucidation of two crystal structures of a known inhibitor series containing this motif confirmed that fragment screening can correctly identify the optimal binding positions of suitable molecules. Although the cinnamic acid moiety alone binds with very modest potency ($IC_{50}$ = 130 µ*M*), it is already so well positioned that growing it towards other parts of the binding site does not modify its position, while greatly improving the inhibitor potency ($IC_{50}$ = 17 n*M*). Compound 1 is the most potent Pim-1 inhibitor of this series for which a crystal structure is now available. The molecular basis for its high binding affinity was elucidated and will facilitate the development of further improved Pim-1 inhibitors.

We thank Proteros Biosciences for cloning and for initial expression, purification and crystallization protocols, Anne Sparmann for excellent technical support with protein purification and ITC measurements, Ivonne Herms for advice on

Pim-1 crystallization, Petra Helfrich for fermentation, Daniela Henschel for kinase-assay development, the beamline scientists at BESSY, Berlin for help during data collection, Wolfgang Höhne and Andreas Herrmann for support, and Simon Holton and Ursula Egner for critical reading of the manuscript.

## References


Abad-Zapatero, C. & Metz, J. T. (2005). *Drug Discov. Today*, **10**, 464–469.

Bamborough, P., Drewry, D., Harper, G., Smith, G. K. & Schneider, K. (2008). *J. Med. Chem.* **51**, 7898–7914.

Böhm, H.-J. (1992*a*). *J. Comput. Aided Mol. Des.* **6**, 61–78.

Böhm, H.-J. (1992*b*). *J. Comput. Aided Mol. Des.* **6**, 593–606.

Breuer, M., Slebos, R., Verbeek, S., van Lohuizen, M., Wientjens, E. & Berns, A. (1989). *Nature (London)*, **340**, 61–63.

Bullock, A. N., Debreczeni, J., Amos, A. L., Knapp, S. & Turk, B. E. (2005). *J. Biol. Chem.* **280**, 41675–41682.

Bullock, A. N., Debreczeni, J. É., Fedorov, O. Y., Nelson, A., Marsden, B. D. & Knapp, S. (2005). *J. Med. Chem.* **48**, 7604–7614.

Bullock, A. N., Russo, S., Amos, A., Pagano, N., Bregman, H., Debreczeni, J. É., Lee, W. H., von Delft, F., Meggers, E. & Knapp, S. (2009). *PLoS One*, **4**, e7112.

Cheney, I. W., Yan, S., Appleby, T., Walker, H., Vo, T., Yao, N., Hamatake, R., Hong, Z. & Wu, J. Z. (2007). *Bioorg. Med. Chem. Lett.* **17**, 1679–1683.

Ciulli, A. & Abell, C. (2007). *Curr. Opin. Biotechnol.* **18**, 489–496.

Collaborative Computational Project, Number 4 (1994). *Acta Cryst.* D**50**, 760–763.

Congreve, M., Chessari, G., Tisi, D. & Woodhead, A. J. (2008). *J. Med. Chem.* **51**, 3661–3680.

Cuypers, H. T., Selten, G., Quint, W., Zijlstra, M., Maandag, E. R., Boelens, W., van Wezenbeek, P., Melief, C. & Berns, A. (1984). *Cell*, **37**, 141–150.

Dhanasekaran, S. M., Barrette, T. R., Ghosh, D., Shah, R., Varambally, S., Kurachi, K., Pienta, K. J., Rubin, M. A. & Chinnaiyan, A. M. (2001). *Nature (London)*, **412**, 822–826.

Emsley, P. & Cowtan, K. (2004). *Acta Cryst.* D**60**, 2126–2132.

Fedorov, O., Marsden, B., Pogacic, V., Rellos, P., Muller, S., Bullock, A. N., Schwaller, J., Sundstrom, M. & Knapp, S. (2007). *Proc. Natl Acad. Sci. USA*, **104**, 20523–20528.

Fischer, M. & Hubbard, R. E. (2009). *Mol. Interv.* **9**, 22–30.

Geschwindner, S., Olsson, L. L., Albert, J. S., Deinum, J., Edwards, P. D., de Beer, T. & Folmer, R. H. (2007). *J. Med. Chem.* **50**, 5903–5911.

Jacobs, M. D., Black, J., Futer, O., Swenson, L., Hare, B., Fleming, M. & Saxena, K. (2005). *J. Biol. Chem.* **280**, 13728–13734.

Johnson, L. N. (2009). *Q. Rev. Biophys.* **42**, 1–40.

Knighton, D. R., Zheng, J. H., Ten Eyck, L. F., Xuong, N.-H., Taylor, S. S. & Sowadski, J. M. (1991). *Science*, **253**, 414–420.

Kumar, A., Mandiyan, V., Suzuki, Y., Zhang, C., Rice, J., Tsai, J., Artis, D. R., Ibrahim, P. & Bremer, R. (2005). *J. Mol. Biol.* **348**, 183–193.

Lilly, M. & Kraft, A. (1997). *Cancer Res.* **57**, 5348–5355.

Lohuizen, M. van, Verbeek, S., Krimpenfort, P., Domen, J., Saris, C., Radaszkiewicz, T. & Berns, A. (1989). *Cell*, **56**, 673–682.

Lucking, U., Siemeister, G., Schafer, M., Briem, H., Kruger, M., Lienau, P. & Jautelat, R. (2007). *ChemMedChem*, **2**, 63–77.

Minor, W., Cymborowski, M., Otwinowski, Z. & Chruszcz, M. (2006). *Acta Cryst.* D**62**, 859–866.

Morwick, T. M., Prokopowicz, A. S. & Mao, W. (2008). Patent WO/2008/022164.

Murshudov, G. N., Vagin, A. A. & Dodson, E. J. (1997). *Acta Cryst.* D**53**, 240–255.

Olsson, T. S., Williams, M. A., Pitt, W. R. & Ladbury, J. E. (2008). *J. Mol. Biol.* **384**, 1002–1017.

Pagano, N., Maksimoska, J., Bregman, H., Williams, D. S., Webster, R. D., Xue, F. & Meggers, E. (2007). *Org. Biomol. Chem.* **5**, 1218–1227.

Pierce, A. C., Jacobs, M. & Stuver-Moody, C. (2008). *J. Med. Chem.* **51**, 1972–1975.

Qian, K. *et al.* (2009). *J. Med. Chem.* **52**, 1814–1827.

Qian, K. C., Studts, J., Wang, L., Barringer, K., Kronkaitis, A., Peng, C., Baptiste, A., LaFrance, R., Mische, S. & Farmer, B. (2005). *Acta Cryst.* F**61**, 96–99.

Qian, K. C., Wang, L., Hickey, E. R., Studts, J., Barringer, K., Peng, C., Kronkaitis, A., Li, J., White, A., Mische, S. & Farmer, B. (2005). *J. Biol. Chem.* **280**, 6130–6137.

Rarey, M., Kramer, B., Lengauer, T. & Klebe, G. (1996). *J. Mol. Biol.* **261**, 470–489.

Schulz, M. N. & Hubbard, R. E. (2009). *Curr. Opin. Pharmacol.* **9**, 615–621.

Schüttelkopf, A. W. & van Aalten, D. M. F. (2004). *Acta Cryst.* D**60**, 1355–1363.

Shafer, C. M., Lindvall, M., Bellamacina, C., Gesner, T. G., Yabannavar, A., Jia, W., Lin, S. & Walter, A. (2008). *Bioorg. Med. Chem. Lett.* **18**, 4482–4485.

Shuker, S. B., Hajduk, P. J., Meadows, R. P. & Fesik, S. W. (1996). *Science*, **274**, 1531–1534.

Stahura, F. L., Xue, L., Godden, J. W. & Bajorath, J. (1999). *J. Mol. Graph. Model.* **17**, 1–9.

Valdman, A., Fang, X., Pang, S.-T., Ekman, P. & Egevad, L. (2004). *Prostate*, **60**, 367–371.

Weiss, M. S., Brandl, M., Sühnel, J., Pal, D. & Hilgenfeld, R. (2001). *Trends Biochem. Sci.* **26**, 521–523.